Motion Control and Fall Detection of Intelligent Cane Robot

Toshio Fukuda, Jian Huang*, Pei Di, and Kosuge Sekiyama

[1] Key Laboratory of Image Processing and Intelligent Control, School of Automation, Huazhong University of Science and Technology, No. 1037, Luoyu Road, 430074 Wuhan, Hubei, China
[2] Department of Micro-Nano Systems Engineering, Nagoya University, Furo-cho, Chikusa-ku, Nagoya 464-8603, Japan
huang_jan@mail.hust.edu.cn

Abstract. An intelligent cane robot was designed for aiding the elderly and handicapped people walking. The robot consists of a stick, a group of sensors and an omni-directional basis driven by three Swedish wheels. Multiple sensors were used to recognize the user's "walking intention", which is quantitatively described by a new concept called intentional direction (ITD). Based on the guidance of filtered ITD, a novel intention-based admittance motion control (IBAC) scheme was proposed for the cane robot. The experiment results demonstrated that the user feels more natural and comfortable when walking with the assistance of cane robot controlled by the IBAC strategy. To detect the fall of user, a detection method based on Dubois possibility theory was proposed using the combined sensor information from force sensors and a laser ranger finder (LRF) fixed on the cane robot. The human fall model was represented in a two-dimensional space, where the relative position between the Zero-Moment-Point (ZMP) and the center of support triangle was utilized as a significant feature. The effectiveness of proposed fall detection method was also confirmed by experiments.

Keywords: Intelligent Cane Robot, Intention Estimation, Admittance Control, Fall Detection, Zero Moment Point (ZMP), Possibility Theory.

1 Introduction

The world is facing challenges of rapid aging population. Elderly people may suffer from low levels of physical strength due to muscle weakness, which affects

* This work was supported by the International Science & Technology Cooperation Program of China "Precision Manufacturing Technology and Equipment for Metal Parts" under Grant No.2012DFG70640, the International Science & Technology Cooperation Program of Hubei Province "Joint Research on Green Smart Walking Assistance Rehabilitant Robot" under Grant No. 2012IHA00601 and was supported by Program for New Century Excellent Talents in University (Grant No.NCET-12-0214).

S. Mohammed et al. (eds.), *Intelligent Assistive Robots*,
Springer Tracts in Advanced Robotics 106, DOI: 10.1007/978-3-319-12922-8_12

their motion ability significantly. Restricted movement lowers the performance of most activities of daily living (ADLs). In addition, the growing elderly population causes the shortage of young people for nursing care. Therefore, walking-aid robots find their application in the nursing and therapy field for these mobility impaired people.

A number of walking-aid robots have been proposed in the last decade, including RT-Walker, PAMM, and so on. So far, the walking-aid robot systems may be mainly classified into two groups according to mobility factor, i.e., the system moving on the ground according to the motion of the subjects and the system giving effects of walking to the subjects. The former system is active-type walker [1] [2] which is driven by servo motor. The latter corresponds to a system driven by servo brakes and is passive-type walker [3] [4]. There is still much space for improvement of the present walker systems. First, most walkers can only be used in the indoor environment. Second, the cumbersome design makes them be difficult to operate by novices. In addition, many old persons are not so weak that they have to be nursed carefully. Moderate support, like a cane or stick, is sufficient to help them go outside and improve their ADL functioning to a great extent. In this sense, a robot cane system may be more useful than walkers due to its flexibility and handiness.

Spenko proposed the well-known PAMM system in [5] together with a Smartcane robot. This cane robot has relative small size but the nonholonomic kinematics reduces its maneuverability. To make the cane robot can be used in most of the living environment (e.g. the narrow corridor, the elevator etc.), an omni-directional moving ability is required. Recently, commercial omni-wheels are available and applied in the area of walker systems[6]. Based on the wheels, small omni-directional platform can be constructed. In this article, an intelligent cane system was proposed and investigated based on a commercially available three-wheeled omni-directional platform.

2 Mechanical Design of Intelligent Cane Robot

The intelligent cane robot system consists of several parts: a tiltable metal stick, an omni-directional base, a control subsystem, and a group of sensors.

The tilt mechanism of metal stick is realized by two servo motors whose rotation axes are perpendicular to each other (see Fig. 1). By rotating the two motor, the stick can tilt to any direction. This may improve the stability of cane robot when a fall event suddenly occurs.

The omni-directional base is comprised of three commercial omni-wheels and the corresponding actuators. The resultant moving velocity is confined less than 1.2m/sec so as to ensure the safety of user. Despite the small size, the load capacity of this mobile base is up to 50 kilograms.

In the sensor group, a six-axis force sensor is mounted at the end of stick to measure the interaction forces between the robot and the user. The walking intention of user can be inferred from the measured forces, which will be illustrated in Section 3. Two laser ranger finders (LRFs) are used to measure the distances

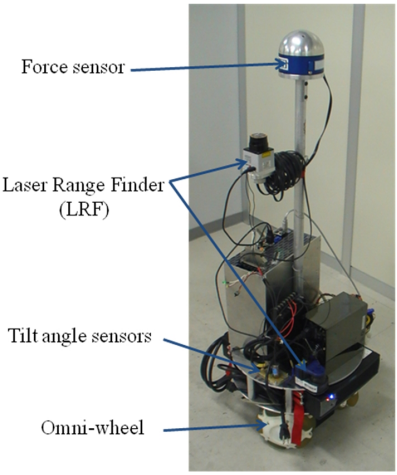

Fig. 1. The intelligent cane robot system

between the stick and the legs, and between the stick and the body, respectively. By online sampling the distance information, fall-prevention function of the cane robot may be implemented as Hirata did in [7].

3 Walking Intention Based Motion Control of Intelligent Cane Robot

3.1 Modeling and Estimation of Human Walking Intention

Preliminary Definitions and Force Analysis. The coordinate definition of human-cane robot system is shown by Fig. 2, in which the coordinate system $O - x_1y_1z_1$ is the reference frame. The local coordinate system $O - x_ry_rz_r$ is fixed on the cane robot and rotates with the yaw angle ψ. The coordinate system $O - x_Iy_Iz_I$ is related to the intentional direction, which is illustrated in the following.

To control the cane robot in accordance with the user's intention, it is necessary to quantify and formulate the human walking intention. Therefore, an important concept called "Intentional Direction (ITD)" is proposed in our previous work [8] to comply with this requirement.

Definition 1. *The direction to which a person intends to move is referred to as intentional direction (ITD).*

As illustrated by Fig. 2, the ITD is not always parallel to the sagittal plane because there are various possible walking modes, including lateral moving, turning around etc.. Note that the ITD can be evaluated by the angle between the forward direction (FW) and the ITD itself. $\rho(n)$ is used to denote the time-variant ITD in the rest of the paper. Here n is the time scale.

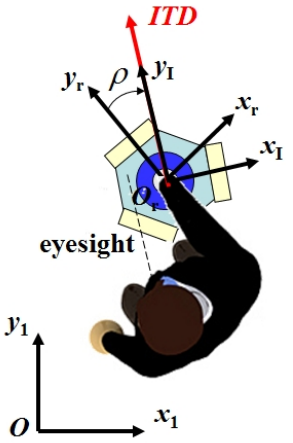

Fig. 2. Quantitative representation of the intentional direction (ITD). The eyesight line is denoted by the broken line, which indicates the direction that the user is intentional to move.

During the user's walking aided by the cane robot, the measured force and torque at time n are denoted by $\mathbf{F}(\mathbf{n})$ and $\mathbf{n}(\mathbf{n})$. The measurement can be represented in different coordinate systems as follows:

$$\begin{cases} \mathbf{F}(n) = \left[{}^{r}F_x(n)\ {}^{r}F_y(n)\ {}^{r}F_z(n)\right]_r^T = \left[{}^{I}F_x(n)\ {}^{I}F_y(n)\ {}^{I}F_z(n)\right]_I^T, \\ \mathbf{n}(n) = \left[{}^{r}n_x(n)\ {}^{r}n_y(n)\ {}^{r}n_z(n)\right]_r^T = \left[{}^{I}n_x(n)\ {}^{I}n_y(n)\ {}^{I}n_z(n)\right]_I^T \end{cases} \tag{1}$$

Except the direction, the quantity of this intention is characterized by the absolute value of measured resultant force ${}^{I}F_y(n)$ along the ITD.

State Model of ITD. The dynamic model of ITD is required to obtain the quantitative formulation of the user's walking intention. Since the dynamics of ITD has different forms in different walking modes, we first enumerate all possible walking modes. Because only several modes are often used in the daily life, the enumeration procedure can be simplified. In this study, we are concerned about five simple walking modes, which are listed in TABLE 1. The transition diagram of the five modes is also illustrated in Fig.3.

To detect the transition between any two walking modes, the following assumptions are concluded from common experiences.

Assumption 1. *In mode I, the ITD is supposed to be always zero.*

Assumption 2. *In mode II, the ITD is supposed to be a constant.*

Assumption 3. *In mode III, the ITD monotone converges to zero from an initial non-zero value.*

Table 1. POSSIBLE WALKING MODES

Mode	Description
I	Stop
IIa	Go straight forward
IIb	Go straight in other directions
IIIa	Turn to the right
IIIb	Turn to the left

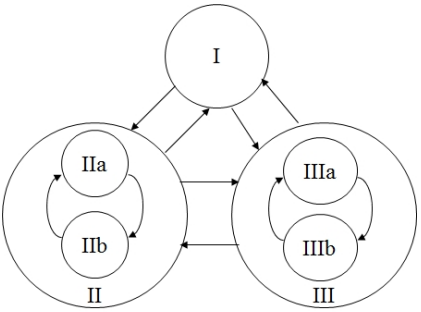

Fig. 3. Transition diagram of possible walking modes

Normally, there is some target one wants to move towards during turning around. Assumption 3 is then proposed based on this fact (see Fig. 4). During the process of turning around, the value of $\rho(n)$ decreases gradually and finally converges to zero, which causes a transition to mode I or II.

According to these assumptions and the proposed walking modes, a hybrid linear state model of ITD can be obtained as follows:

$$\rho(n+1) = A_{\sigma(n)} \cdot \rho(n), \quad \sigma(n) \in \{I, II, III\} \tag{2}$$

where $\sigma(n)$ is used to denote the different walking mode given by TABLE 1. The state transition matrices are given by

$$A_I = 0, A_{II} = 1, A_{III} = a(n) \tag{3}$$

where $a(n)$ satisfies

$$0 < a(n) < 1 \tag{4}$$

Observation Model of ITD. Note that the state variable $\rho(n)$ cannot be directly measured. The interaction forces between the user and cane robot reflect the walking intention. Obviously, the ITD is along the direction of resultant force of F_x and F_y if there are no measurement noises. Thus, the observation model of ITD is described by

$$y(n) = \tan^{-1}\left(\frac{{}^{r}F_x(n)}{{}^{r}F_y(n)}\right) = \rho(n) + \omega(n) \tag{5}$$

$\omega(n)$ is a combination of sensor noises and human gait habit. Normally, different people have different gait habit during walking (e.g., some people unintentionally move laterally even when they walk straight forward). For the sake of simplicity, $\omega(n)$ is assumed as a white noise sequence with a user-dependent covariance $Q(\rho)$. It is observed that the values of $Q(\rho)$ are almost same for the same user. Thus, conventional Kalman filter is very suitable for estimating the ITD in mode II and III.

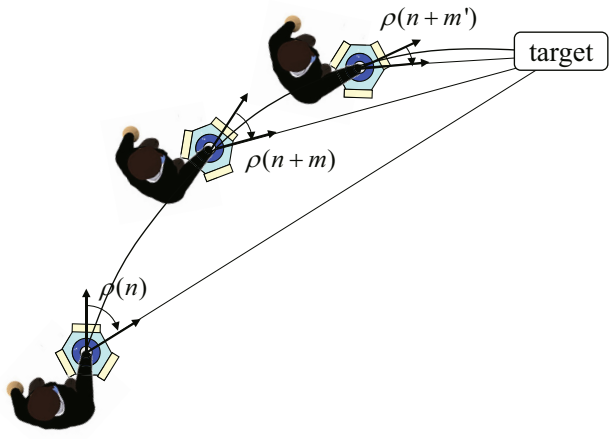

Fig. 4. Typical turning around move mode

Online Estimation of ITD Based on Kalman Filters. In this section, we discuss the approach to online estimate the ITD from measured forces. The first problem that should be solved is how to detect the walking mode transition. In this study, we use a rule-based method to infer current walking mode $\sigma(n)$. Fuzzy threshold detection methods are used to check if some rule is satisfied. These rules are generated from common-sense experiences and described as follows.

Rule set. (Rule-Based Method)

1. IF $\sigma(n-1) \neq$ I AND ${}^{r}F_x(n) \approx 0$ AND ${}^{r}F_y(n) \approx 0$ AND ${}^{r}n_z(n) \approx 0$, THEN $\sigma(n) =$ I.
2. IF $\sigma(n-1) \neq$ IIa AND ${}^{r}F_x(n) \approx 0$ AND $|{}^{r}F_y(n)| > 0$ AND ${}^{r}n_z(n) \approx 0$, THEN $\sigma(n) =$ IIa
3. IF $\sigma(n-1) \neq$ IIb AND $|{}^{r}F_x(n)| > 0$ AND $|{}^{r}F_y(n)| > 0$ AND ${}^{r}n_z(n) \approx 0$, THEN $\sigma(n) =$ IIb
4. IF $\sigma(n-1) \neq$ IIIa AND ${}^{r}n_z(n) > 0$, THEN $\sigma(n) =$ IIIa
5. IF $\sigma(n-1) \neq$ IIIb AND ${}^{r}n_z(n) < 0$, THEN $\sigma(n) =$ IIIb

In mode I and II, the dynamics of ITD is described by a linear state model. Therefore a conventional Kalman filter is suitable to be applied to online estimate the ITD.

In mode III, the state model of ITD can be rewritten as

$$\rho(n+1) = (a_0 + \Delta a(n)) \cdot \rho(n) \tag{6}$$

where a_0 is a constant and satisfies $0 < a_0 < 1$. $\Delta a(n)$ is the model uncertainty. It is well known that normal Kalman filter will generally not guarantee satisfactory performance when uncertainty exists in the system model. Thus, we choose a robust Kalman filter to calculate the estimation of ITD in this case [9].

We conclude the above discussion by proposing the following online ITD estimation algorithm.

Algorithm 1. (Online ITD Estimation Algorithm)
Input: $\mathbf{F}(n-1)$, $\mathbf{n}(n-1)$, $y(n)$, $\rho_e(n-1)$, $\sigma(n-1)$

1. Apply the rule-based method to determine $\sigma(n)$
2. IF $\sigma(n-1) = \sigma(n)$ THEN
3. SWITCH $\sigma(n)$
4. CASE I:Let $\rho_e(n) = 0$
5. CASE II:
6. Use the Kalman filter to infer $\rho_e(n)$
7. IF $\sigma(n) =$ IIa THEN let $\rho_e(n) = 0$
8. CASE III:
9. Use the robust Kalman filter to infer $\rho_e(n)$
10. ELSE
11. Let $\rho_e(n) = y(n)$ to initialize the filter.
12. ENDIF

Output: $\rho_e(n)$, $\sigma(n)$

3.2 Walking Intention Based Admittance Control

The cane robot motion controller uses an admittance control scheme based on the inferred human intention, which is called intention based admittance control (IBAC) scheme. The conventional admittance control uses an admittance model emulates a dynamic system and gives the user a feeling as if he is interacting with the system specified by the model. This model is defined as a transfer function with the users forces and toques, F(s), as the input and the reference velocity of cane robot, V(s), as the output. It is expressed as:

$$G(s) = \frac{V(s)}{F(s)} = \frac{1}{Ms + B} \tag{7}$$

where M and B are the mass and damping parameters respectively.

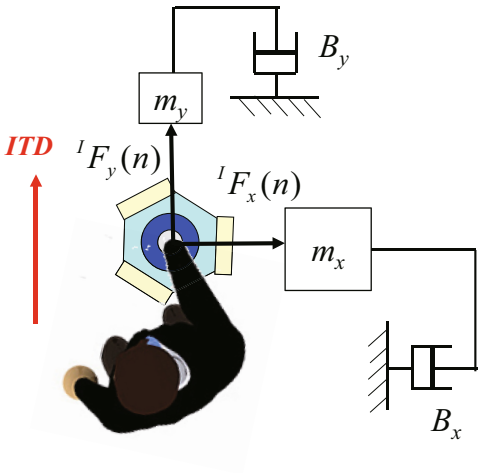

Fig. 5. The principle of IBAC scheme

During walking, people feel comfortable if the cane is easily maneuvered in the ITD and hardly maneuvered in the direction perpendicular to the ITD. To meet the requirement, we propose the IBAC scheme in which two admittance models are used. One model is defined for the motion along the ITD, which has selected mass and damping parameters from the acceptable area presented in [5]. The other model is defined for the motion perpendicular to the ITD, which has much bigger mass and damping parameters. The general idea is shown by Fig. 5. The final three-DOF mass-damping model for our cane robot is defined as:

$$\mathbf{M}^d \cdot \ddot{\mathbf{q}}^d + \mathbf{B}^d \cdot \dot{\mathbf{q}}^d = \mathbf{F} \tag{8}$$

where state $\mathbf{q}^d$ and the measured force $\mathbf{F}$ are represented in the coordinate frame $\{I\}$ based on the current walking intention, satisfying

$$\mathbf{q}^d = \begin{bmatrix} {}^I x^d \\ {}^I y^d \\ {}^I \rho^d \end{bmatrix}_I, \mathbf{F} = \begin{bmatrix} {}^I F_x \\ {}^I F_y \\ n_z \end{bmatrix}_I \tag{9}$$

Matrices $\mathbf{M^d}$ and $\mathbf{B^d}$ are the desired mass and damping coefficients. These coefficients are described by

$$\mathbf{M^d} = \begin{bmatrix} {M_x}^d & 0 & 0 \\ 0 & {M_y}^d & 0 \\ 0 & 0 & {J_z}^d \end{bmatrix}, \mathbf{B^d} = \begin{bmatrix} {B_x}^d & 0 & 0 \\ 0 & {B_y}^d & 0 \\ 0 & 0 & {B_z}^d \end{bmatrix} \tag{10}$$

where ${M_x}^d >> {M_y}^d, {J_z}^d$and ${B_x}^d >> {B_y}^d, {B_z}^d$

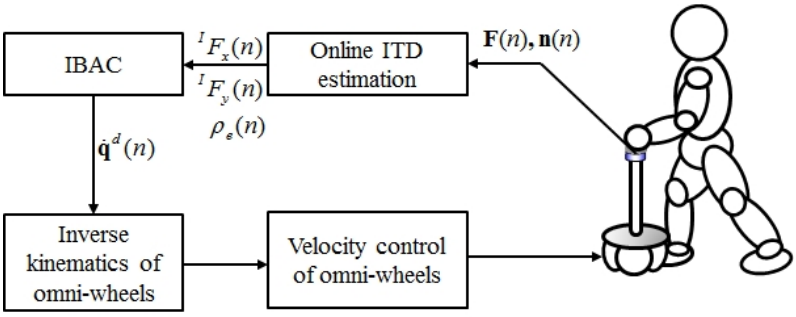

Fig. 6. Control diagram of the whole system

3.3 Experiment Study

Investigating Observation Noise. Three university students (subject A, B and C) utilized the cane robot realizing mode II and III in these experiments. Same experiments were performed by them while wearing the brace to imitate a handicapped people. To verify the white noise assumption of the observation noise, firstly the subjects were requested to intentionally maneuver the robot moving straight along five fixed directions, which is shown by Fig. 7. From these experiments, we can investigate the observation noise characteristics of ITD by applying statistic techniques. For moving-straight experiments (mode II), the observation noise $\omega(n)$ can be easily obtained and analyzed from the observation model (5). For the obtained noise signal of each experiment, we tested both the normality and independence of residuals by applying Jarque Bera and Portmanteau test methods. It was found that more than 80% of the experiment results passed the statistical tests. Thus, a white noise assumption is thought to be acceptable in our study.

Further, the results of evaluated covariance Q of the white observation noise $\omega(n)$ are also depicted in Fig. 7. For each subject, the direction-dependent Q of this subject can be thought as a random variable. Coefficients of variation (cv) of these random variables were calculated and found to be less than 10%. Therefore, it is reasonable to assume that values of Q are almost the same in different directions for the same person, as pointed out in subsection B of section III. Another interesting phenomenon that should be pointed out is that the covariance Q of the subject wearing a brace is higher than that of the subject performing a normal walking. This proves the fact that the observation noise of a handicapped peoples walking is usually bigger than that of a normal people.

Motion Control on Flat Ground. In the experiments for illustrating the validity of the IBAC control strategy, subject A utilized the cane robot to implement two series of walking modes.

The inferred ITDs and their observations based on force signals are shown in Fig. 8(a) and Fig. 9(a). Trajectories of estimated mode are also shown in

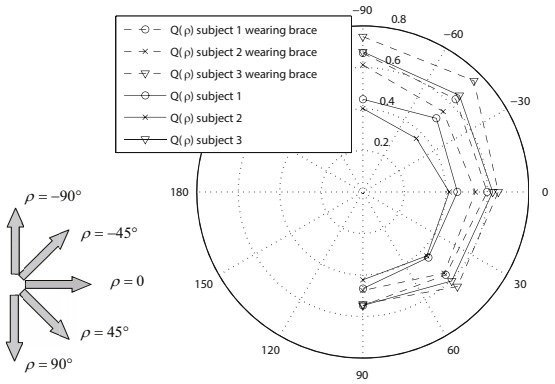

Fig. 7. The covariance of noise when a person moves straight

these figures, where we use integers from 1 to 5 to denote the five walking modes sequentially (see the value of mode trajectory depicted by the dot-dash line). Note that even if there are some fault recognitions of mode transition, the performance of rule-based mode transition function is sufficiently satisfactory in the practice. In the experiment results, the main fault recognitions of mode transitions are mistaking mode IIa for mode IIb. This will not affect the system performance much because mode IIa is actually a special case of mode IIb. The advantage of fast detection of mode IIa is to quickly get an accurate ITD estimation ($\rho_e(n) = 0$), which can be used to guide the motion control very clearly. However, even mode IIa is mistaken for mode IIb, the ITD which is estimated by Kalman filter is nearly equal to zero and smooth enough to obtain a satisfactory intention-based motion control.

As mentioned above, Kalman filter and robust Kalman filter are used in mode II and III respectively. Coefficient $a(n)$ in model (3) satisfies $a(n) = a_0 + \Delta a(n)$ with $a_0 = 0.93$, $|\Delta a(n)| < 0.3$. Comparing with the observation $y(k)$ from the noisy force signals, the online estimated ITD $\rho_e(n)$ reflects the human intention smoothly and distinctly, which provides explicit guidance to the IBAC controller. In particular, when the subject moves straight forward, which is the walking mode in most of the time, the inferred ITD is exactly the forward direction. This reduces meaningless lateral movements of the cane robot to a great extent. In addition, typical force responses are shown in Fig. 8(b) and Fig. 9(b) of the walking experiments.

Comparison Experiment Study. As illustrated in section V.A, observation noise of the ITD always exists while the cane robot is operated by either a normal user or an imitated disabled user. If a conventional force control approach is applied, the cane robot will move unexpectedly due to the effect of noise. This unexpected motion makes the user feel uncomfortable and deteriorates

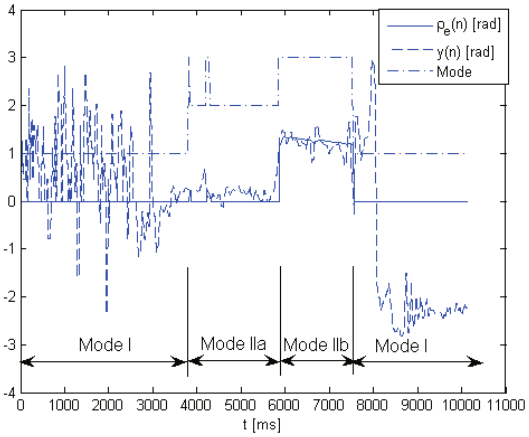

(a) Observed and inferred ITD vs Time (ms)

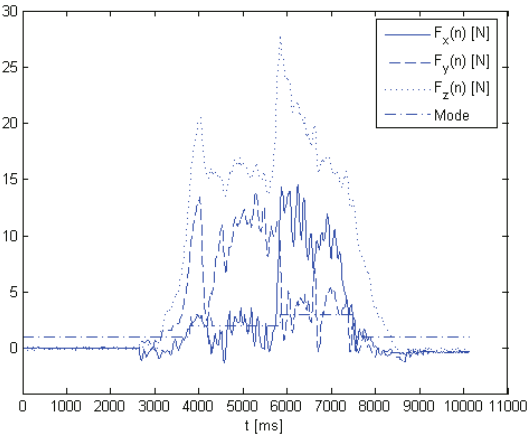

(b) Force signals vs Time (ms)

Fig. 8. Experiment 1 on the flat ground (I→IIa→IIb→I)

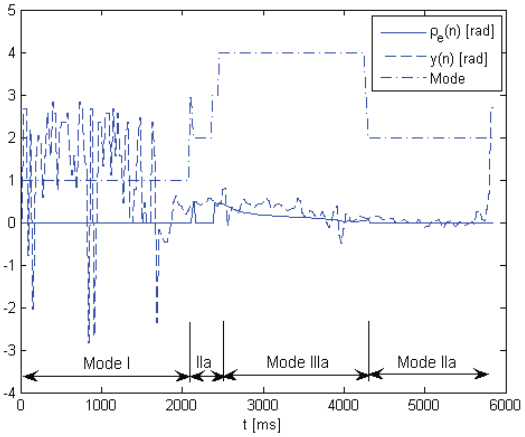

(a) Observed and inferred ITD vs Time (ms)

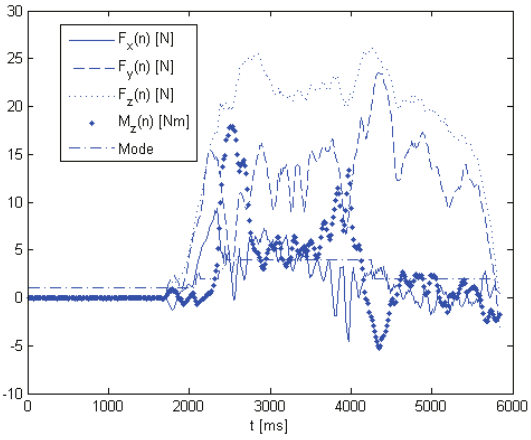

(b) Force signals vs Time (ms)

Fig. 9. Experiment 2 on the flat ground (I→IIa→IIIa→IIa)

the maneuverability of robot. To safely assist the elderly or disabled walking, the proposed IBAC approach overcomes the disadvantage of conventional force control to a great extent. The validity of IBAC approach is further illustrated by the following experimental comparison study.

In this experiment, a subject was asked to perform two series of walking modes depicted by Fig. 10. A conventional admittance control (CAC) strategy which is often used in [5] was tested first and the motion trajectories of cane robot were recorded. The same experiments were conducted on the cane robot controlled by the IBAC strategy.

To quantitatively evaluate the coincidence between the motion of cane robot and the users walking intention, we assume a metric which is given by

$$D(cane, ITD) = \frac{1}{N} \sum_{i=1}^{N} \sqrt{(x_c(i) - x_{fit}(i))^2 + (y_c(i) - y_{fit}(i))^2} \qquad (11)$$

where N is the data number of a motion trajectory of cane robot. $(x_c(i), y_c(i))$ is the i-th point in the motion trajectory. $(x_{fit}(i), y_{fit}(i))$ is the i-th point of the best-fit line through the point set of the motion trajectory. Note that the best-fit line should be obtained according to the given walking mode series, which reflect the users walking intention. For instance, the best-fit line of walking experiment A (see Fig. 10(a) consists of two straight lines representing the walking mode IIa and IIb respectively. The best-fit line of walking experiment B (see Fig. 10-(b) is composed of two straight lines (representing mode IIa at the beginning and end of the walking mode series) and an arc (representing mode IIIa).

Fig. 11 shows two comparison results of walking experiments on flat ground using the IBAC strategy and the conventional admittance control strategy. The difference between the robot motion trajectory in the case of using the IBAC strategy and its best-fit line is much smaller than that in the case of using normal admittance control. This fact was further proven by calculating the average values of *D(cane,ITD)* after conducting a number of comparison experiments in different cases illustrated in the above subsections (see Table 2). As a conclusion, smaller values of *D(cane,ITD)* are obtained when the IBAC strategy is applied to our cane robot. That is, there are less unexpected motions of the cane robot if the IBAC strategy is employed. This is very important in the sense of making the user feel safe and comfortable while operating the cane robot.

Table 2. Comparison of $D(cane, ITD)$ using different control strategies

Subject	Experiment number	Average Value of D (CAC)	Average Value of D (IBAC)
A	50	0.0129	0.006
B	50	0.0117	0.006

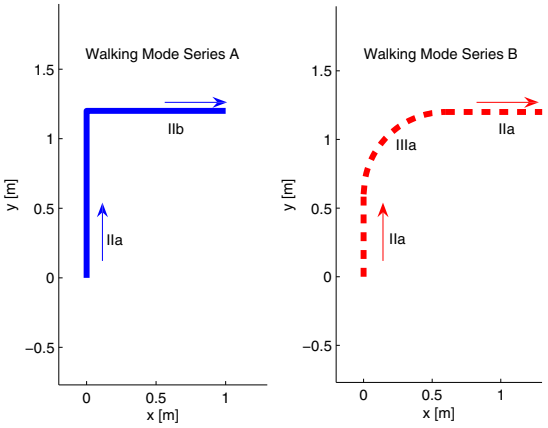

(a) (b)

Fig. 10. Two walking mode series used in the comparison study

4 Fall Detection Using Intelligent Cane Robot

4.1 ZMP Estimation

In this study, a novel method is proposed to detect the risk of falling in the elderly based on Zero-Moment-Point (ZMP) estimation. The ZMP is a very important concept of the motion planning for biped robots, and also can be applied in the area of tripedal or multiped robot. There are two walking modes of legged robot from a stability viewpoint; one is statically stable walking and the other is dynamically stable walking. For dynamically stable walking robot, the ZMP can be computed using the equations (12), (13). The stability can be achieved by controlling the position of ZMP of the robot to be inside the support polygon.

$$x_{zmp} = \frac{\sum_{i=1}^{n} m_i x_i \left(\ddot{z}_i + g\right) - \sum_{i=1}^{n} m_i \ddot{x}_i z_i - \sum_{i=1}^{n} I_{iy} \ddot{\theta}_{iy}}{\sum_{i=1}^{n} m_i \left(\ddot{z}_i + g\right)} \tag{12}$$

$$y_{zmp} = \frac{\sum_{i=1}^{n} m_i y_i \left(\ddot{z}_i + g\right) - \sum_{i=1}^{n} m_i \ddot{y}_i z_i - \sum_{i=1}^{n} I_{ix} \ddot{\theta}_{ix}}{\sum_{i=1}^{n} m_i \left(\ddot{z}_i + g\right)} \tag{13}$$

where m_i is the mass of link, I_{ix}, I_{iy} are the inertial components, θ_{ix}, θ_{iy} are the acceleration of link (as shown in Fig. 12).

Unfortunately, these equations can only be used to compute the ZMP for a robot system, not for a human. Since the human is an uncontrollable factor in

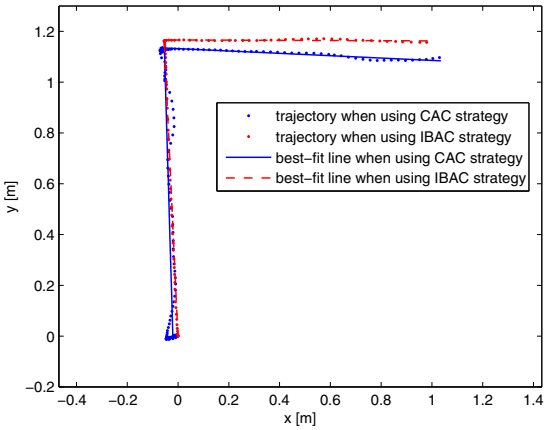

(a) A comparison of experiment results for walking mode series A

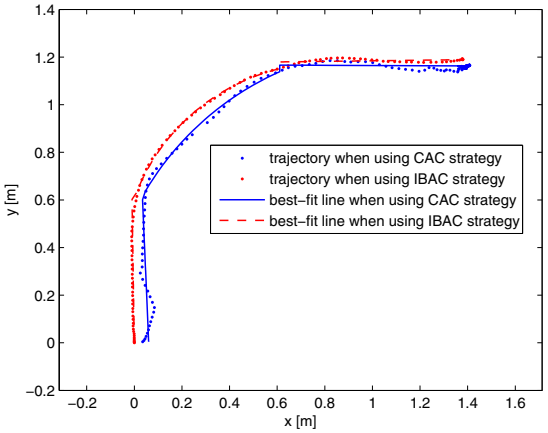

(b) A comparison of experiment results for walking mode series B

Fig. 11. Comparisons of experiment results using the IBAC strategy and the CAC strategy

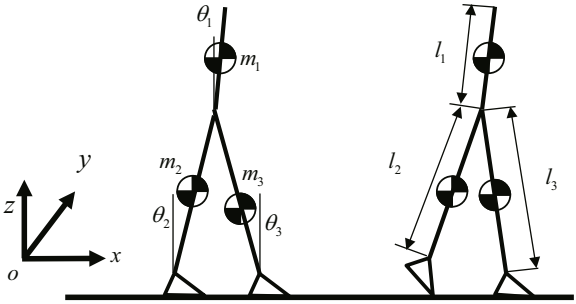

Fig. 12. The simplified link model of human walking

our human-cane system, we cannot control the movement and rotation of each part of human body. Furthermore, the position of each link (x_i, y_i, z_i) cannot be obtained by the existing sensors of the cane robot system. Therefore, we cannot control or even estimate the ZMP of user by using Eq. (12), (13).

Thus, the statically stable walking model is applied to estimate the users ZMP. The static model can remain statically stable if and only if its center of gravity (COG) projects vertically inside the support polygon. In a quasi-static case, the ZMP is proved be equivalent to the projection of COG. According to this principle, the falling risk can be detected by the statically walking model given by

$$x_{cog} = \frac{\sum_{i=1}^{n} x_i f_i}{\sum_{i=1}^{n} f_i}, \; y_{cog} = \frac{\sum_{i=1}^{n} y_i f_i}{\sum_{i=1}^{n} f_i} \tag{14}$$

where x_i, y_i (n=1, 2, 3) denote the position of ground reaction force (the LRF is origin of the coordinate system). f_i denotes the magnitude of ground reaction force measured by the 6-axis force sensor and on-shoe load sensor that will be illustrated as follows.

4.2 Sensor Configuration

To apply the statically mode model (14), a wearable load sensor system was proposed to obtain the dynamical ground reaction force. This system includes four parts which is shown in Fig. 13-(A).

As shown in Fig. 14, the ground reaction forces f_1, f_2 and f_3 are measured by the 6-axis force sensor and on-shoe load sensors respectively. The three contact points are denoted by P_1, P_2 and P_3. The coordinate value of point P_1, is easily obtained for it is just the position of cane robot. By using a laser ranger finder, the coordinate values of point P_2 and P_3 can be approximately calculated (see the two yellow scanned segments on the legs in Fig. 14).

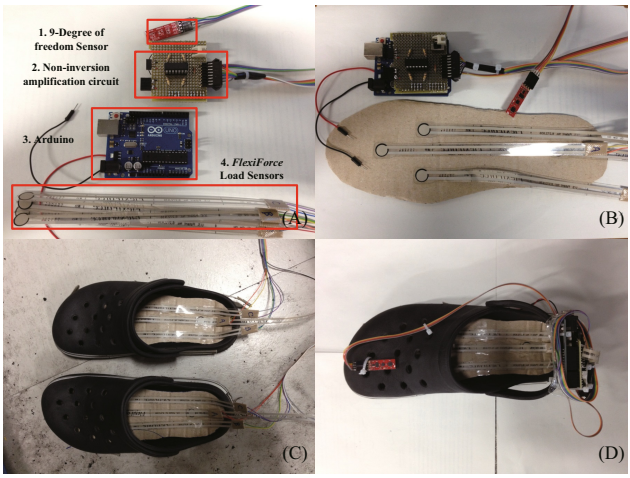

Fig. 13. On-shoe load sensor system

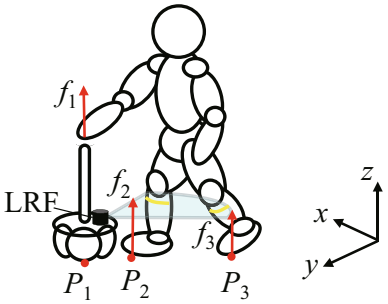

Fig. 14. Sensory data required in ZMP estimation

4.3 Fall Detection Method Based on Fuzzy Theory

As shown in Fig. 15-(a), possible falling states include 'forward falling', 'backward falling' and 'sideward falling'. Here state 'sideward falling' consists of all falling cases except forward and backward falling. In Fig. 15-(b), the positions of point P_1, P_2, P_3 and ZMP are depicted for all possible falling cases.

Obviously, an important feature indicating the user's falling state is the relative position between the ZMP and point P_0, which is the center of support triangle with vertices P_1, P_2 and P_3 (see Fig. 16). This relative position can be described by a two-dimensional vector $(\Delta x, \Delta y)^T$. While the user is walking normally, the ZMP should fluctuate around P_0 in a small area. This area differs from different people. When the user is falling down, the distance between ZMP and P_0 will increase suddenly. And the falling direction can also be easily obtained by observing vector $(\Delta x, \Delta y)^T$.

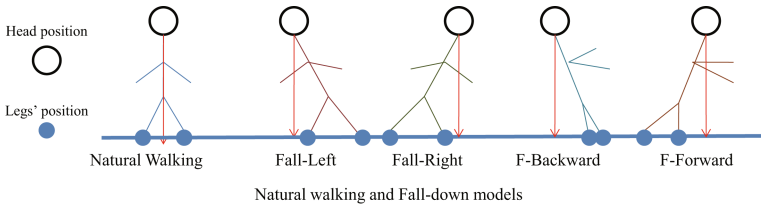

(a) Normal walking and possible falling states

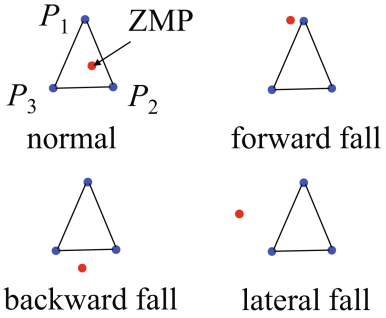

(b) Point positions of different falling cases

Fig. 15. Walking states analysis

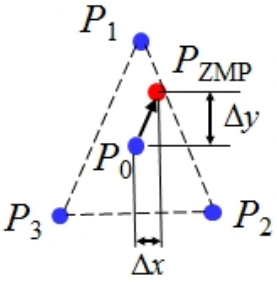

Fig. 16. The feature $(\Delta x, \Delta y)^T$ of fall detection

The distribution of feature during normal walking is analyzed similar to [7]. Dubois possibility theory is applied to describe the distribution of vector $\overrightarrow{P_0 P_{ZMP}} = [\Delta x, \Delta y]^T$ during the normal walking state [10].

The procedure starts by constructing the data histograms for Δx and Δy^T during normal walking state. The number of bins h for a histogram is experimentally determined. Each bin is represented by the center of the interval denoted by y_j. The height of each bar is the number of learning points, located in this bin.

The probability distribution $\{p(y_j) : \ j = 1, 2, \cdots, h\}$ is calculated by dividing the height of each bin by the total number of learning points belonging to the

same class. The possibility distribution $\{\pi(y_j) : \ j = 1, 2, \cdots, h\}$ is deduced from the probability distribution by the bijective transformation of Dubois and Prade defined by

$$\pi(y_k) = \sum_{j=1}^{h} \min\left[p(y_k), p(y_j)\right] \tag{15}$$

The membership functions $\mu(\cdot)$ that characterize the fuzzy set "normal walking", is finally calculated from the corresponding possibility distributions by linear interpolation.

The fall detection is implemented by a very simple algorithm, which is illustrated as follows: (assuming the human walking behavior is monitored at discrete times, n denotes the current time)

IF $\mu(\Delta x(n), \Delta y(n)) < c$ *and* $\mu(\Delta x(n-1), \Delta y(n-1)) < c$, *THEN a fall is detected.*

Constant c is a small positive number which indicates a very low possibility of "normal walking" state.

4.4 Experiment Study

We experimented with the cane robot to illustrate the effectiveness of the proposed methods. First, the possibility distribution of "normal walking" state is investigated. Then the validity of fall detection method is verified by experiments.

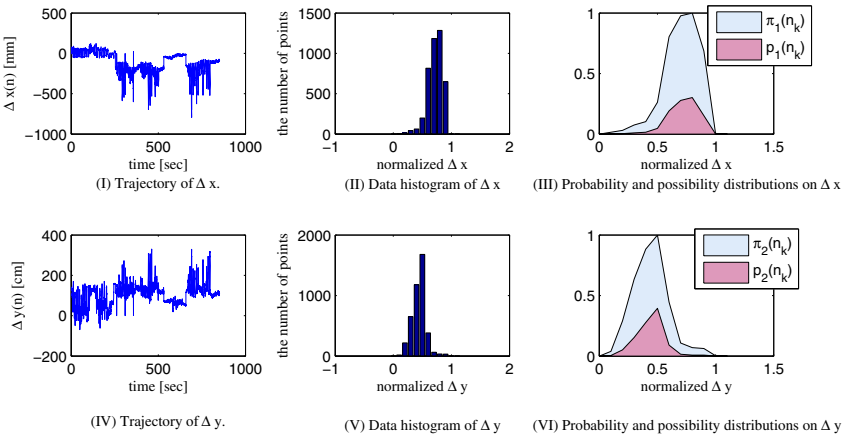

Fig. 17. Trajectories, data histagrams, probability and possibility distributions of "normal walking

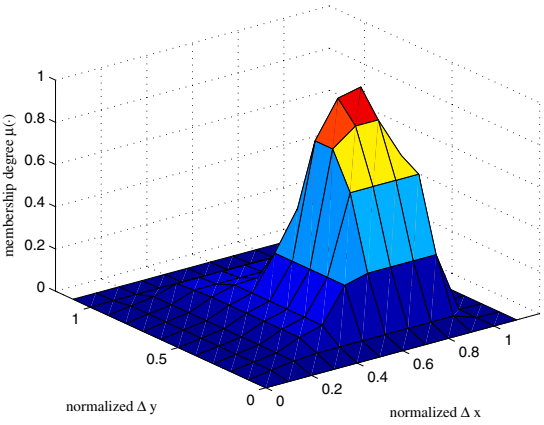

Fig. 18. The membership degree function of "normal walking"

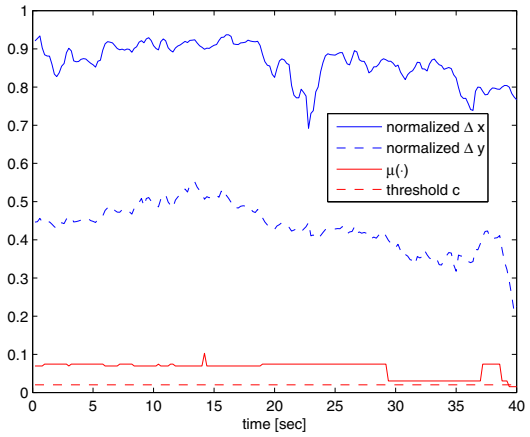

Fig. 19. Fall detection experiment

Experiments of "Normal Walking". A university students were requested to operate the cane robot to conduct "normal walking" experiments. From the experimental data, the possibility distributions of "normal walking" were obtained as well as the membership degree function. The original trajectories and corresponding data histograms of $\Delta x(n)$ and $\Delta y(n)$ are shown in Fig. 17 (I) and (IV). The constant h is assumed to be 10. The probability distribution $p(n_k)$, possibility distribution $\pi(n_k)$ are depicted in Fig. 17 (II), (III), (V) and (VI). The obtained membership function $\mu(\Delta x(n), \Delta y(n))$ is given in Fig. 18

Experiments of "Fall Detection". In this experiment, the subject pretended to fall down during walking. The fall detection rule described in section 4.3 was

applied in the experiment. Constant c was chosen as 0.02. The fall was detected promptly as shown by Fig. 19.

4.5 Conclusion

A new omni-directional type intelligent cane robot is developed for the elderly and handicapped. Motion control and fall detection of this robot are studied based on online estimating human walking intention and the position of ZMP.

The main contribution of this study lies in: 1) presenting dynamic models and online inference algorithm for the human walking intention, which is significant to lead the user walking in a natural and comfortable way. 2) proposing practical ZMP based fall detection method during operating the cane robot. An intention based admittance control (IBAC) scheme is also proposed and used to drive cane robot. Experiments were performed on the flat ground to verify the effectiveness of proposed algorithms.

Future work will focus on the investigation of fall prevention measures and plentiful operation experiments by different users.

References

1. Dubowsky, S., Genot, F., Godding, S.K., Skwersky, H.A., et al.: PAMM-a robotic aid to the elderly for mobility assistance and monitoring: A helping-hand for the elderly. In: IEEE International Conference on Robotics and Automation, pp. 570–576. IEEE Press, New York (2000)
2. Hirata, Y., Baba, T., Kosuge, K.: Motion control of omni-directional type walking support system walking helper. In: The 12th IEEE International Workshop on Robot and Human Interactive Communication (RO-MAN), pp. 85–90. IEEE Press, New York (2003)
3. Rentschler, A.J., Cooper, R.A., Blaschm, B., Boninger, M.L.: Intelligent walkers for the elderly performance and safety testing of vapamaid robotic walker. Journal of Rehabilitation Research and Development 40, 423–432 (2003)
4. Hirata, Y., Hara, A., Kosuge, K.: Passive-type intelligent walking support system "RT Walker". In: IEEE International Conference on Intelligent Robots and Systems (IROS), pp. 3871–3876. IEEE Press, New York (2004)
5. Yu, H., Spenko, M., Dubowsky, S.: An Adaptive Shared Control System for an Intelligent Mobility Aid for the Elderly. Auton. Robots 15(1), 53–66 (2003)
6. Soai Co. Ltd., `http://www.soai-net.co.jp/`
7. Hirata, Y., Muraki, A., Kosuge, K.: Motion Control of Intelligent Passive-type Walker for Fall-prevention Function based on Estimation of User State. In: IEEE International Conference on Robotics and Automation (ICRA), pp. 3498–3503. IEEE Press, New York (2006)
8. Wakita, K., Huang, J., Di, P., Fukuda, T., Sekiyama, K.: Human Walking Intention Based Motion Control of Omni-directional Type Cane Robot. IEEE/ASME Trans. Mechtronics 18(1), 285–296 (2013)
9. Xie, L., Soh, Y.C., Souza, C.E.: Robust Kalman Filtering for Uncertain Discrete-time Systems. IEEE Trans. Automat. Contr. 39(6), 1310–1314 (1994)
10. Dubois, S., Prade, H.: Possibility Theory and Its Applications: A Retrospective and Prospective View. In: IEEE International Conference on Fussy Systems, pp. 25–28. IEEE Press, New York (2003)